Delft University of Technology

Structural Health and Stability Assessment of High-Speed Railways via Thermal Dilation Mapping With Time-Series InSAR Analysis

Qin, Xiaoqiong; Liao, Mingsheng; Zhang, L; Yang, Mengshi

Citation (APA)
Qin, X., Liao, M., Zhang, L., & Yang, M. (2017). Structural Health and Stability Assessment of High-Speed Railways via Thermal Dilation Mapping With Time-Series InSAR Analysis. *IEEE Journal of Selected Topics in Applied Earth Observations and Remote Sensing*, *10*(6), 2999 - 3010 . https://doi.org/10.1109/JSTARS.2017.2719025

Important note
To cite this publication, please use the final published version (if applicable).
Please check the document version above.

Structural Health and Stability Assessment of High-speed Railways via Thermal Dilation Mapping with Time-Series InSAR Analysis

Xiaoqiong Qin, Mingsheng Liao, Lu Zhang, Mengshi Yang

Abstract—**Thermal dilation is a vital component of deformation along the extensive railway network infrastructure. To monitor subtle deformation, Synthetic Aperture Radar Interferometry (InSAR) technique has been adopted as a space-borne geodetic tool. However, InSAR applications in railway stability surveillance have been largely limited by the sparseness of detectable point-like targets (PTs). Moreover, only one-dimensional linear displacements in radar line-of-sight direction can be measured by a single data stack. To address these issues, we developed an improved Persistent Scatterers InSAR approach that can retrieve thermal dilation effects with an increased number of PTs along the railways. This proposed strategy effectively combines SAR amplitude, interferometric phase, and the spatial information of railway structures to maximize the number of PTs. A least square fitting of the residual phase obtained by iterative spatial-temporal filtering with respect to temperature difference is used to estimate the thermal dilation of metal and concrete-asphalt materials. To validate the effectiveness of this approach, case studies using ENVISAT ASAR (ASAR) and TerraSAR-X (TSX) datasets were carried out on the Railways of Beijing-Tianjin, Beijing-Shanghai, and Shanghai-Hangzhou. Subsidence velocity, gradient, and thermal dilation were used to identify hazardous grades along each railway. Furthermore, linear deformation rates in two dimensions, i.e. vertical and west-east directions, along Shanghai-Hangzhou Railway were inverted from ascending ASAR and descending TSX observations to reveal track conditions at a high level of detail.**

Index Terms—**High-speed railway, thermal dilation, gradient, risk assessment**

I. INTRODUCTION

OVER the past decade, China has massively expanded the national high-speed railway network. The Beijing-Tianjin

X. Qin and L. Zhang are with State Key Laboratory of Information Engineering in Surveying, Mapping and Remote Sensing (LESMARS), Wuhan University, Wuhan 430079, China (e-mail: qinxiaoqiong@whu.edu.cn).

M. Liao is with LESMARS and Collaborative Innovation Center of Geospatial Technology, Wuhan University, Wuhan 430079, China, and Key Laboratory of Land Subsidence Monitoring and Prevention, Ministry of Land and Resources, Shanghai 200072, China (e-mail: liao@whu.edu.cn).

M. Yang is with LESMARS, Wuhan University, Wuhan 430079, China, and Department of Geoscience and Remote Sensing, Delft University of Technology, 2628 CN Delft, The Netherlands.

Railway (JJR), the Beijing-Shanghai Railway (JHR), and the Shanghai-Hangzhou Railway (HHR) are essential elements in China's "Four Vertical and Four Horizontal" Passenger Line Network. Uneven regional subsidence expansion, however, may change the tracks geometry, and poses great threats to the stability of railways. According to the design specifications of national high-speed railways, when the speed reaches 300 km/h, the maximum allowable differential settlement of 100 m along the track must be controlled to within 20 mm, limiting the maximum slope to 20‰ [1]-[2]. Lack of timely effective deformation monitoring may lead to major accidents if the accumulated deformation is beyond the prescribed limits. Consequently, monitoring the structural health and stability of high-speed railways is essential for transportation safety.

For many years, high-speed railways relied on conventional on-structure measurements conducted annually or only after potentially damaging incidents. Currently, a high dense survey network does not exist and surveys are prohibitively expensive. Given these limitations, monitoring such linear infrastructures at a large scale requires new kinds of enabling technologies. Synthetic Aperture Radar Interferometry (InSAR) technique provides a precise and efficient tool to measure progressive surface deformation over wide areas with an extremely low cost [3]-[6]. It offers the potential for all-time working capabilities without interference in routine operations, which is a considerable benefit for the busy routes. Based on the conventional InSAR, various time-series InSAR techniques were developed to overcome the intrinsic limitations of temporal/spatial decorrelation and atmospheric disturbances [7]-[10]. As manmade linear tracks often maintain stable backscattering over a long time, time-series InSAR technologies facilitate the monitoring of long-span tracks at millimeter level accuracy with high spatial resolution [11]-[13]. Although many studies have been carried out in this research field, from an application point of view, the existing time-series InSAR approaches are still limited by the sparseness of detectable point-like targets (PTs) in decorrelated areas. At the same time, only one-dimensional linear displacements in the radar line-of-sight (LOS) direction can be measured by a single data stack. These two issues are especially of concern when monitoring high-speed railways in outskirts.

Besides conventional linear deformation, the thermal dilation also accounts for a significant portion of the total deformation [14]-[15]. To determine the current conditions of

the railways, an improved Persistent Scatterers InSAR (PSI) approach is proposed to retrieve the thermal dilation effects with an increased number of PTs. A strategy that effectively combines SAR amplitude, interferometric phase, and the spatial information of railway structure is employed to maximize the number of PTs. The PTs for subsequent analysis are identified in two areas: the local area exactly along the route and surrounding area with a five km buffer zone. A least square fitting of the residual phase obtained by iterative spatial-temporal filtering with respect to temperature difference is used to estimate the thermal dilation of metal and concrete-asphalt materials. The linear subsidence velocity, gradient, and thermal dilation were used to identify the hazardous grades along high-speed railways. Furthermore, linear deformation rates in two dimensions (vertical and west-east directions) along the HHR were inverted from the ascending ENVISAT ASAR (ASAR) and descending TerraSAR-X (TSX) observations to reveal track conditions at a high level of detail. This paper aims to provide useful reference for the structural health and stability assessment of high-speed railways, thus informing operators whether the track is in an acceptable condition or is suffering from gradual damage.

II. STUDY AREA AND DATA

The JJR and JHR are the earliest and the longest high-speed railways in China respectively. The HHR, with the biggest railway station (Hongqiao Railway Station) in the route, is the fastest railway in China. From the perspective of engineering geology, they are located on the vulnerable compressible alluvial plains in the eastern coastal area of China where the ground subsidence has always been one of the most severe and widespread geological hazards [16]-[17]. Although land subsidence generally evolves very slowly, the uneven subsidence along tracks would still result in huge security risks.

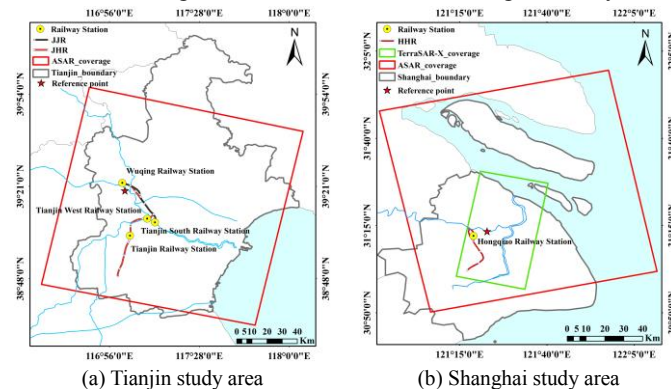(a) Tianjin study area   (b) Shanghai study area

Fig. 1. Study areas. (a) Coverage of ASAR images (red rectangle), JJR and JHR are marked by black and red line. (b) Coverage of TSX (green rectangle) and ASAR images (red rectangle), HHR is marked by a red line. The reference points are highlighted by red stars.

In this study, 17 ascending ASAR images from 2008 to 2009 in Tianjin with large coverage of 100×100 km^2 are used to monitor the deformation long the JJR and JHR (see Fig. 1(a) and Table I). Moreover, three stacks including 20 descending TSX images from 2008 to 2010, 15 descending TSX images

from 2011 to 2012, and 24 ascending ASAR images from 2008 to 2010 are collected to extract the deformation of the HHR (see Fig. 1(b), Table. II, and Table. III).

TABLE I
BASIC INFORMATION FOR ASAR DATASET IN TIANJIN

No.	Acquisition Date	No.	Acquisition Date
1	20080208	10	20090123
2	20080314	11	20090227
3	20080418	12	20090508
4	20080523	13	20090612
5	20080627	14	20090717
6	20080801	15	20090821
7	20080905	16	20091030
8	20081010	17	20091204
9	20081219		

TABLE II
BASIC INFORMATION FOR TSX DATASETS IN SHANGHAI

No. (2008-2010)	Acquisition Date	No. (2011-2012)	Acquisition Date
1	20080421	1	20110916
2	20080820	2	20111008
3	20090328	3	20111030
4	20090408	4	20111121
5	20090419	5	20111213
6	20090511	6	20120104
7	20090522	7	20120206
8	20090602	8	20120310
9	20090624	9	20120401
10	20090829	10	20120515
11	20090920	11	20120628
12	20091012	12	20120720
13	20091023	13	20120811
14	20091114	14	20120902
15	20091206	15	20121005
16	20091217		
17	20091228		
18	20100108		
19	20100119		
20	20100130		

TABLE III
BASIC INFORMATION FOR ASAR DATASET IN SHANGHAI

No.	Acquisition Date	No.	Acquisition Date
1	20080107	13	20090302
2	20080211	14	20090406
3	20080317	15	20090511
4	20080421	16	20090720
5	20080526	17	20090824
6	20080630	18	20090928
7	20080804	19	20091102
8	20080908	20	20091207
9	20081013	21	20100111
10	20081117	22	20100215
11	20081222	23	20100426
12	20090126	24	20100531

III. METHODOLOGY FOR HIGH-SPEED RAILWAY MONITORING

An improved PSI analysis approach is applied in this study (see Fig. 2.), which can be divided into three parts: the data input layer, the data processing layer and the result interpretation layer. In the data input layer, all the available information such as time-series SAR images, temperature, the spatial information of rails, and the expert knowledge (the maximum allowable differential settlement and slopes, and hazard grading standards) are collected for data processing and interpretation. In the data processing layer, the spatial information is considered in PT identification and a least square fitting is used in thermal dilation estimation in order to enhance the accuracy and reliability of the measurements. In the results interpretation layer, the two-dimensional linear deformation rates along the HHR inverted from ascending and descending SAR observations were verified by previous studies or cross validation. The distribution characteristics and mechanisms of thermal dilation were investigated and verified by the physical properties of materials. Finally, hazard grades were evaluated along the rails. Three main improvements of our method are elaborated in the following.
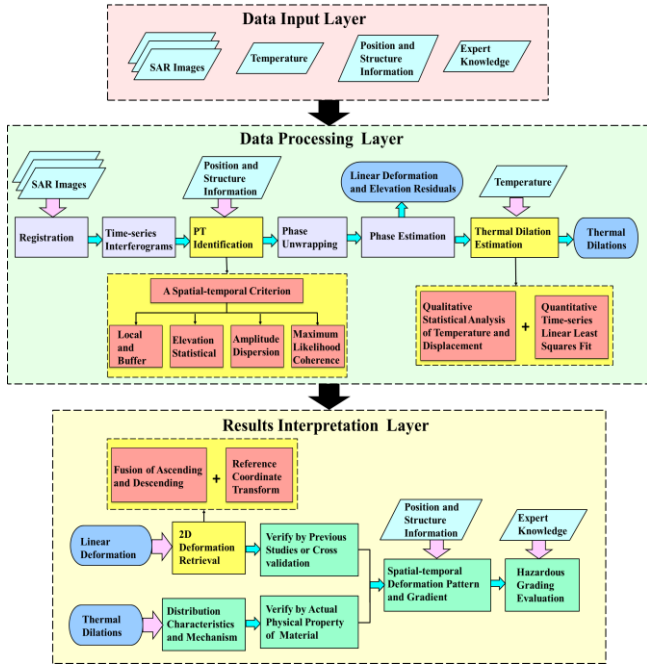

Fig. 2. Workflow of improved PS-InSAR method

A. Point Targets Detection

Since our purpose is to estimate the subsidence parameters of high-speed railways, we focus our attention on identifying and analyzing PTs associated with the tracks.

From the co-registered SLCs, we accurately select the stable PTs on the tracks by a spatial-temporal strategy. Firstly, in the temporal domain, a set of points with multi-temporal amplitude stability and high backscattering intensity throughout the observation period are considered as PT candidates. Then, maximum likelihood of coherence γ_m, expressed as Eq. (1), is used to evaluate the phase stability for each points [18]-[19].

$$\gamma_m = \frac{1}{N}\left|\sum_{i=1}^{N} exp\{j(\emptyset_{int} - \widetilde{\emptyset}_{int} - \Delta\widehat{\emptyset}_{\theta})\}\right| \quad (1)$$

Here N is the number of available interferograms. $\emptyset_{int}$ indicates the interferometric phase, $\widetilde{\emptyset}_{int}$ denotes the filtered spatial correlated parts and $\Delta\widehat{\emptyset}_{\theta}$ represents the look angle error. The PT candidates are selected based on the theoretical of probabilistic distribution. A γ^* is used to identify a maximum number of measured points while keeping the false alarm rate below a given value q which is the maximum fraction of all the selected pixels that will be accepted as non-PT pixels [18]. The γ^* can be calculated by Eq. (2) where $\alpha \in [0,1]$ is the proportion of a candidate being a PT. $p(\gamma_m)$ and $p'(\gamma_m)$ are the probability density functions of being a PT or a random phase pixel. The ensemble coherence values are used as a threshold to select pixels for which $\gamma_m > \gamma^*$ as PTs. Finally, two candidate subsets based on amplitude and coherence are combined together to maximize the density of PTs.

$$\frac{(1-\alpha)\int_{\gamma^*}^{1} p'(\gamma_m)d_{\gamma^*}}{\int_{\gamma^*}^{1} p(\gamma_m)d_{\gamma^*}} = q \quad (2)$$

Spatially, points falling outside of the buffer zone along high-speed railways are excluded. After estimating the subsidence rates and elevation residuals of the PTs, a statistical analysis of the PTs is carried out to get a local reasonable elevation range based on the assumption that the elevation of points along the track should be successive. Therefore, a point should be filtered when its elevation exceeds three times of the standard deviation of its surrounding points.

B. Thermal Dilation Estimation

After removing the topographic phase with SRTM, the differential phase $\emptyset_{diff}$ can be considered as the sum of four components with respect to a given reference point:

$$\emptyset_{diff}(i) = \emptyset_{def}(i) + \emptyset_{topoerr}(i) + \emptyset_{atm}(i) + \emptyset_{res}(i) \quad (3)$$

Where $\emptyset_{def}$ indicates the phase related to linear deformation of PT i in the LOS direction, $\emptyset_{topoerr}$ denotes the phase associated to the height error, $\emptyset_{atm}$ means the phase due to the fluctuations of water vapor in the atmosphere and $\emptyset_{res}$ includes the thermal dilations, look angel error, system noise and so on [20]. Then, PTs within a given distance were connected to constitute a local network along the railway based on a balance of the computation and validity. In order to reducing the effect of spatially correlated errors, the phase increments between two adjacent PTs i and j in an interferogram are calculated by:

$$\delta\emptyset_{def}(i,j) = \frac{4\pi}{\lambda} \cdot \Delta v \cdot B_t \quad (4)$$

$$\delta\emptyset_{topoerr}(i,j) = \frac{4\pi}{\lambda} \cdot \frac{B_n}{Rsin\theta} \cdot \Delta\varepsilon \quad (5)$$

Here, Δv and $\Delta\varepsilon$ are the velocity and height error increments between neighboring PTs. B_t and B_n are the temporal baseline and spatial normal baseline of the interferogram. λ, R and θ are the wavelength, distance from satellite to target, and incident angle respectively. As the atmospheric perturbation is spatially correlated, the neighboring atmospheric differential phase $\delta\emptyset_{atm}(i,j)$ is supposed to be zero. With differential interferograms of the same area, an iterative weighted least squares adjustment is performed to estimate the topographic error and the linear deformation of all the PTs by (4) and (5). After subtracting the deformation and height error components

from the initial differential interferogram, the rest parts are mainly constituted by the atmosphere phase and residual phase. Particularly, the residual phase of PT i can be decomposed as:

$$\emptyset_{res}(i) = \emptyset_{th}(i) + \emptyset_{\theta}(i) + \emptyset_{noise}(i) \qquad (6)$$

Here $\emptyset_{th}(i)$ indicates the thermal dilation phase, $\emptyset_{\theta}(i)$ denotes the look angel error, and $\emptyset_{noise}(i)$ is noise. There is an approximately linear relationship between $\delta\emptyset_{\theta}$ and $\Delta\theta$. Therefore, the look angel error can be estimated by [18]

$$\delta\emptyset_{\theta} = \lambda/4\pi \, B_n \Delta\theta \qquad (7)$$

According to the empirical model [21], the atmosphere phase and nonlinear thermal dilation phase have different frequency characteristics in the spatial and temporal domain. Under the assumption that in the flat area such as Shanghai and Tianjin, the stratified atmosphere effect is insignificant, only the turbulent atmosphere effect should be taken into consideration [22]. Therefore, for a pixel, the atmosphere conditions at different radar images can be seen as a random process, which means it can be considered as a white noise in the temporal. Meanwhile, it is also a spatially low-frequency signal [20]. However, the thermal dilation represents a small spatial correlation but a low frequency feature in the time domain. Consequently, the atmosphere can be separated by the spatial-temporal filtering.

Finally, our focus turns to the thermal dilation which often affects the survey results, especially for steel or reinforced concrete railway tracks. When the temperature is not available, the thermal dilation was modeled as a periodic function based on a complete seasonal cycle assumption [14]-[15]. When the temperature is available, a third unknown parameter was introduced by extending the interferometric phase model [15]. However, both the above approaches increase the computational burden. Moreover, as PSI technique aims at extracting useful information from the original observations, the separation of thermal dilation had better be considered in the post-processing and interpretation so that it would not affect the previous estimation. In this study, an approach to correlate the residuals with temperature changes by means of least-squares estimation is performed. As the system noise is supposed to be quite small on a given PT with high signal to noise ratio, the $\phi_{res}(i)$ can be approximately considered as a linear function of temperature difference:

$$\begin{cases} \phi_{res}(i) \cdot \frac{\lambda}{4\pi} = \alpha \cdot \Delta \boldsymbol{T} \\ \Delta \boldsymbol{T} = [\Delta T_1, \dots \Delta T_N]^{\mathrm{T}} \end{cases} \qquad (8)$$

With the assumption that temperature is homogeneous along the railway, the temperature deformation parameter (TDP) $\alpha(mm/°C)$ can be accurately estimated by the temperature difference of i th differential interferometry ΔT_i and the residual phase $\phi_{res}(i)$. To validation the linear model of thermal dilation due to the expansion and contraction of material for a given object, it is possible to use the TDP difference $\Delta\alpha$ and thermal expansion magnitude ΔL deducing the thermal expansion coefficient (TEC) c of the material from (9). This estimation is supposed to be consistent with the physical property of the construction material.

$$c = \frac{\Delta\alpha}{\Delta L} \qquad (9)$$

C. Two-dimensional Deformation Retrieval

Due to the oblique scene illumination, a single SAR dataset can only measure the one-dimensional LOS displacements. The generally low incidence angle makes the InSAR measurements mostly sensitive to ground uplift or subsidence, which limits the accurate inversion of real surface deformation [23]. Combining SAR ascending and descending orbits, the two-dimensional displacements (vertical and east-west directions) along the HHR are estimated in this study to reveal its track conditions at a high level of detail[24]-[25].

SAR side-looking geometry is illustrated in Fig. 3, where S and O represent the satellite and target respectively, and θ is the incidence angle. Dashed line $S'O$ is the projection of SO onto the horizontal plane, φ is the angle between $S'O$ and the north direction. Thus, the LOS velocity is the geometric sum of the 3D velocities projected to the LOS direction [23]-[24], which is given by:

$$V_{LOS} = \cos(\theta)V_V + \sin(\theta)\sin\left(\varphi - \frac{3\pi}{2}\right)V_E + \sin(\theta)\cos\left(\varphi - \frac{3\pi}{2}\right)V_N \quad (10)$$

Here V_V, V_E and V_N are the velocities in vertical, west-east, and north-south directions respectively. For ASAR images of the JHR and JJR, θ is 22.8° and φ is -14°, (10) can be written as:

$$V_{LOS} = 0.922V_V - 0.376V_E + 0.094V_N \qquad (11)$$

For TSX images of the HHR, θ is 26.42° and φ is -10°:

$$V_{LOS} = 0.896V_V - 0.436V_E + 0.077V_N \qquad (12)$$

For ASAR images of the HHR, θ is 22.77° and φ is 13.22°:

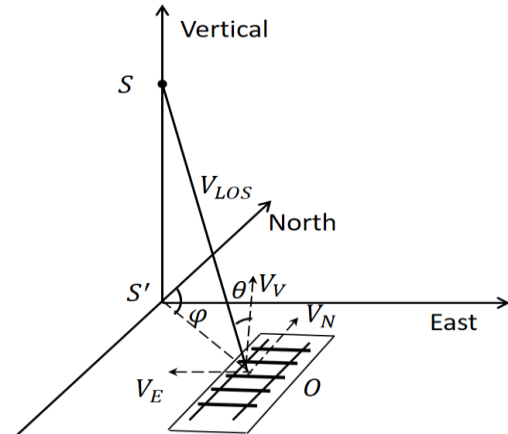$$V_{LOS} = 0.922V_V + 0.377V_E + 0.089V_N \qquad (13)$$

Fig. 3. 3D geometry view of the railway track

Therefore, given the orbit parameters, PSI measurements have the highest sensitivity in the vertical deformation while the lowest sensitivity in the north-south direction. However, estimating the 3D deformation with three unknowns against one LOS measurement is ill-posed. For the JHR and JJR, since no other information for deformation direction is available, we assume that the deformation is dominant in the vertical direction, which is supported by [16]. Then, the velocity of the JHR and JJH can be estimated by:

$$V_V = V_{LOS}/0.922 \qquad (14)$$

For the HHR, we measured the LOS displacements of both ascending and descending orbits and projected the results into the same geographic coordinate system. After correcting by

leveling data, the co-registration of two results is implemented by taking TSX as the main track. Considering the different resolutions, only the common PTs are selected. Specially, a local maximum window filter is used to keep the strong scatterers in both datasets [26]. Moreover, the point-pairs from the two datasets with a distance shift less than 0.1 pixels and an elevation discrepancy within 1 m are treated as the common PTs candidates. Then, the PSI parameter estimates of the common PTs are integrated. Regarding the time span and revisit cycle, although the time spans are not completely identical, we estimated the linear deformation rate of PTs in an overlapping period which should keep a consistent overall trend in a long period.

However, we still can't determine 3D deformation with two measurements unless an additional constraint is introduced. Since the north-south direction with the lowest sensitivity is approximately the longitudinal direction of the HHR where the deformation has the least influence on its safety, we estimate two parameters with an assumption that the deformation is mainly in the vertical and west-east directions. Therefore, for each common PT, our object is to estimate vertical and east-west velocities ($V = [V_V \ V_E]^T$) from the LOS velocities of ascending and descending orbits ($R = [R_A \ R_D]^T$). Thus, the deformation velocities of the HHR can be referenced to a common datum by:

$$R = A \cdot V \tag{15}$$

$$A = \begin{bmatrix} cos\theta_A & sin\theta_A sin(\varphi_A - \frac{3\pi}{2}) \\ cos\theta_D & sin\theta_D sin(\varphi_D - \frac{3\pi}{2}) \end{bmatrix} \tag{16}$$

$$V = [A^T \cdot P \cdot A]^{-1} \cdot A^T \cdot P \cdot R \tag{17}$$

Here **A** is the matrix associated with the SAR observation geometry, and **P** is the weight matrix. Assuming that the measurements from the two datasets are independent, using the standard dispersion ($1/\sigma_{R_A}$, $1/\sigma_{R_D}$) of observations to determine the weight is a simple and effective method.

$$P = \begin{bmatrix} 1/\sigma_{R_A} & 0 \\ 0 & 1/\sigma_{R_D} \end{bmatrix} \tag{18}$$

IV. RESULTS AND INTERPRETATION

Experimental analyses and numerical risk evaluation were carried out to detect the complex subsidence phenomenon with multiple factors along three high-speed railways in this study.

A. Beijing-Tianjin and Beijing-Shanghai High-speed Railway

1) Subsidence Status Along the Route

Based on our method, the linear deformation rate and thermal dilation distribution along the JJR track from 2008 to 2009 are estimated and displayed in Fig. 4(a) and (b) respectively. The track is marked by a black line and stations are highlighted by yellow circles. The track showed heterogeneous deformation with the subsidence velocities from -16 to 4 millimeter per year (mm/yr). An obvious subsidence segment near Shuangjie Town and Yongding New River was identified. Shuangjie Town is an industrial zone where the groundwater pumping yield has dramatically increased as a

result of rapid economic development and industrial modernization [27]-[28]. Consequently, the severe water table depression, due to the excessive exploitation of groundwater, would further lead to interstitial water runoff and aquifer compression accounting for the subsidence damage [29]-[30].
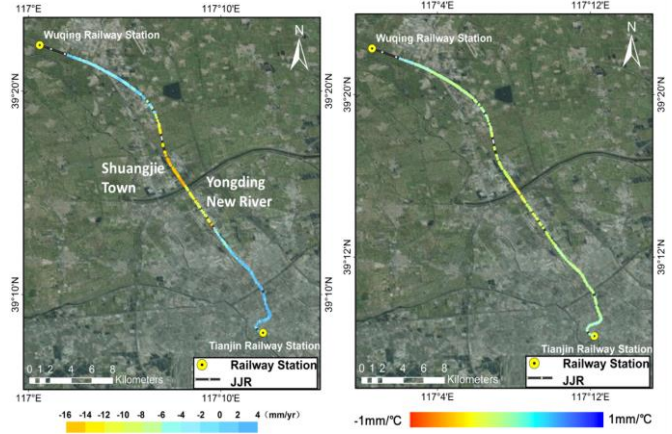
(a) Linear deformation rate   (b) Thermal dilation

Fig. 4. Linear deformation rate and thermal dilation maps of JJR (2008-2009). Background image: Google Map.
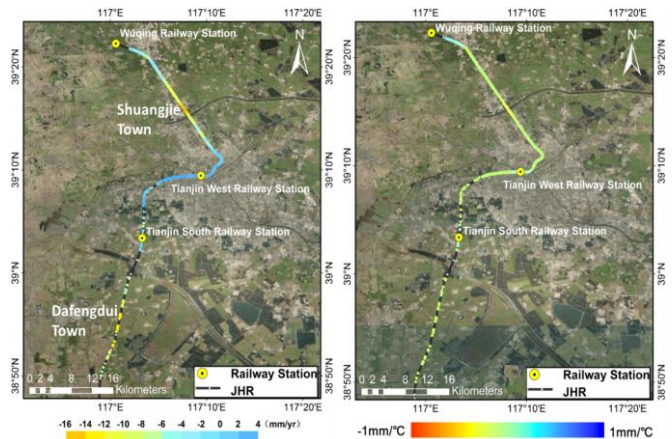
(a) Linear deformation rate   (b) Thermal dilation

Fig. 5. Linear deformation rate and thermal dilation maps of JHR (2008-2009). Background image: Google Map.
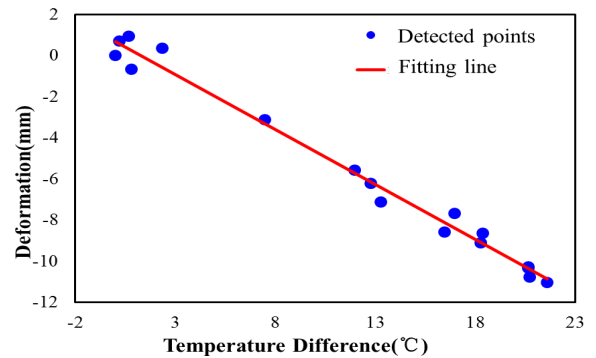

Fig. 6. Scatter plot for residual deformation versus temperature difference of Shuangjie Town segment (2008-2009)

The estimated TDPs are spatially different in Fig. 4(b). Most parts of the track showed a negligible thermal dilation. However, the tracks near Shuangjie Town showed slight thermal dilation up to -0.5 mm/℃. The negative TDPs indicated that there is a slight downward motion in the summer

while a relative upward motion during the winter. As the warmer periods may lead to asphalt subgrade soften and ground water tables decreasing due to the increased temperature and evaporation, the subsidence along the track under the same traffic load would increase. Conversely, the colder periods would harden the asphalt subgrade and raise the ground water tables, enhancing the stability along the route [31].

The linear deformation rate and thermal dilation distribution of the JHR are showed in Fig. 5(a) and (b). The distribution and magnitude of deformation vary spatially, which may probably due to the different consolidated/unconsolidated local situations. Two subsidence centers, Shuangjie Town and Dafengdui Town, along the JHR were identified. Further inspections revealed that the subsidence pattern is highly associated with the local land-use categories. Both the two subsidence centers are located near multiple industrial factories and intensive residential quarters, whereas, the stable sections are occurred in agricultural lands.

The spatial pattern of the TDPs in Fig. 5(b) clearly shows that large parts of the JHR have stable thermal behaviors. However, segments near town areas with industrial factories and residential buildings are more sensitive to the temperature variation. A possible interpretation is that the seasonal variation of asphalt subgrade hardness and groundwater table mentioned above may lead to the negative TDPs. For the other parts of the railway, thermal dilation is not obvious. Taking 10 points on the Shuangjie Town segment as examples, the scatter plot of their average displacements and corresponding temperature differences (see Fig. 6) showed an obvious linear relationship. The root mean square error (RMSE) of the thermal dilation linear fitting model is 1.073 mm.

2) Variation of Subsidence Gradient

A five km buffer zone is established to study more relevant areas that would affect the JJR in Fig. 7(a). A similar subsidence pattern with Fig. 4(a) was found which marked by a white dashed circle, and our results showed the same subsidence pattern with previous studies [27]-[28]. For a detail validation with the previous studies, the statistical maximum, mean, and minimum velocities of Shuangjie Town are compared (see Table VI). The three velocities are close to each other, but with slight deviations. That may because these results are derived by different kinds of datasets. Besides, the observation periods are not exactly the same. Overall, our results agree well with the previous studies no matter in distribution or magnitude.

TABLE VI
PREVIOUS STUDY FOR VALIDATION OF SHUANGJIE TOWN

| Authors	Datasets	Maximum rate (mm/yr)	Mean rate (mm/yr)	Minimum rate (mm/yr)
Keren Dai [27]	TSX	-26	-19	-12
Tao Li [28]	ALOS PALSAR	-20	-15	-10
Our study	ASAR	-24	-18	-12

The uneven subsidence along the railway may change the surface gradient, which would affect the smoothness of the route and the safety of its operation. Deformation difference between neighboring pixels can be described by the subsidence gradient. According to the related calculation method for subsidence gradient along the high-speed railway, within a certain number of years, the subsidence gradient between two points can be calculated by Eq. (19) [32]:

$$g = \Delta d / L = n(v_1 - v_2)/L \qquad (19)$$
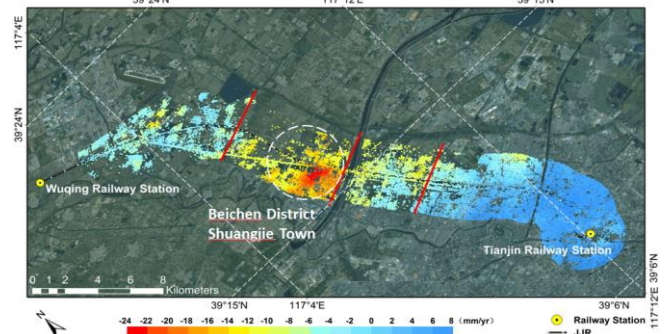
(a) Vertical subsidence rate of the surrounding area with latitude-longitude gridlines overlaid. Background image: Google Map.
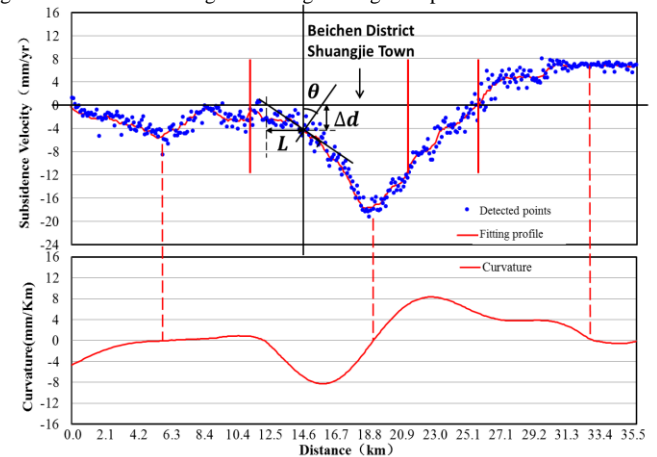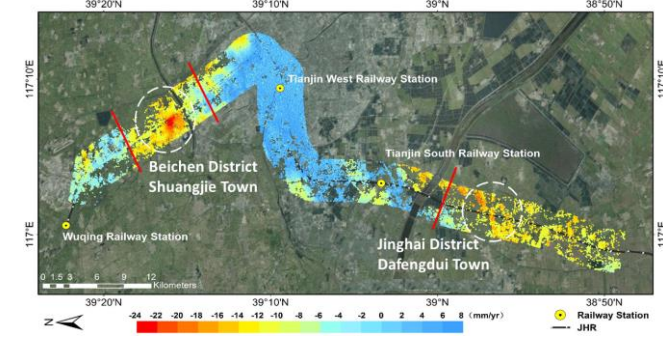

(b) Subsidence rate profile and curvature of JJR

Fig. 7. Vertical subsidence rate, profile and curvature of JJR (2008-2009)

As shown in Fig. 7(b), Δd denotes the ground subsidence difference, L indicates the distance between the two points. n is the number of years, v_1 and v_2 are the subsidence velocities of the two points. When L is infinitely close to zero, the gradient can be substituted by the curvature of subsidence velocity profile. Therefore, we calculated the curvature to analyze the non-uniform subsidence. Assuming that all areas are subsiding at a same level, the high-speed railways would not be threatened by such uniform settlement. However, the uneven ground deformation would play a significant role in the potential hazards, which usually happens not in the subsidence core or non-subsiding area, but just at the edge area of the subsidence bowl. Although the gradient along the JJR is about 0.01‰, which is still within the maximum allowable of 20‰, more attention should be paid to segments with both high subsidence rates and gradients.

An uneven subsiding pattern of the JHR buffer zone, with the subsidence velocity ranging from -24 to 8 mm/yr, was identified in Fig. 8(a). Two apparent subsidence centers marked by white dashed circles, corresponding to the two deep valleys in the vertical deformation rate profile, were observed in Fig.

8(b). Identically, the curvature that reveals the magnitude of gradient along the route is calculated. We can see the zero curvatures situated around the peak subsidence and uplift areas while the local maximum curvatures located near the transition areas of the subsidence and uplift with large subsidence gradients. Therefore, both the deformation rate and gradient should be taken into consideration when evaluating the subsidence status along high-speed railways.

(a) Vertical subsidence velocity of the surrounding area. Background image: Google Map.
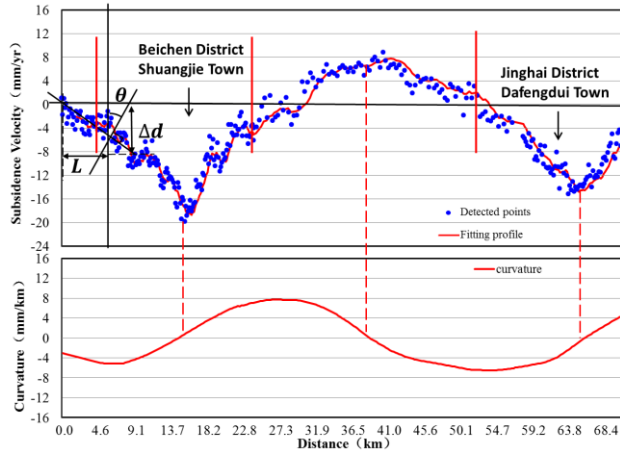
(b) Subsidence rate profile and curvature of JJR

Fig. 8. Vertical subsidence rate, profile and curvature of JHR (2008-2009)

3) Hazardous Grading Evaluation

TABLE V
THE GRADING STANDARDS OF FACTORS FOR TRACK SAFETY EVALUATION

Evaluation factors	Weight	Factor grading	Score
Gradient magnitude (mm/km)	0.6	≥ 4	10
		2~4	5
		≤ 2	1
Subsidence rate(mm/yr)	0.3	≥ 10	10
		4~10	5
		≤ 4	1
TDP (mm/℃)	0.1	≥ 0.3 or ≤ -0.3	10
		$0.1\sim0.3$ or $-0.3\sim-0.1$	5
		≤ 0.1 or ≥ -0.1	1

The deformation of the railway is mainly affected by uneven subsidence expansion, fast ground subsidence growth and thermal dilation effects [32]. Therefore, the subsidence gradient, subsidence rate, and TDP are considered as the main factors for safety evaluation. For comparison, we assign each factor from 1 to 10 based on the factual situation (see Table V). The higher score means higher risk. According to the composite score, the hazardous grades along the JJR and JHR were divided into nine levels in Fig. 9 and Fig. 10.
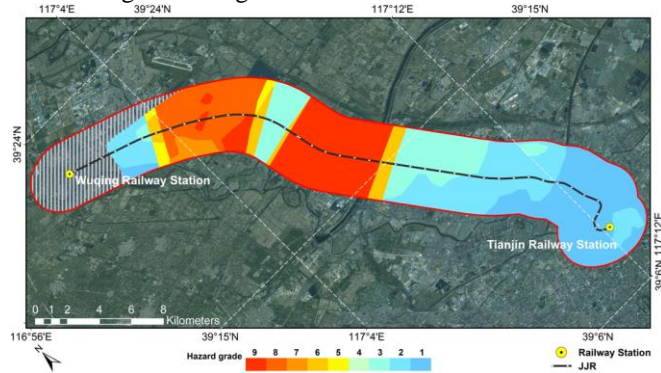

Fig. 9. Hazardous grading of JJR (2008-2009) with latitude-longitude gridlines overlaid. Background image: Google Map.
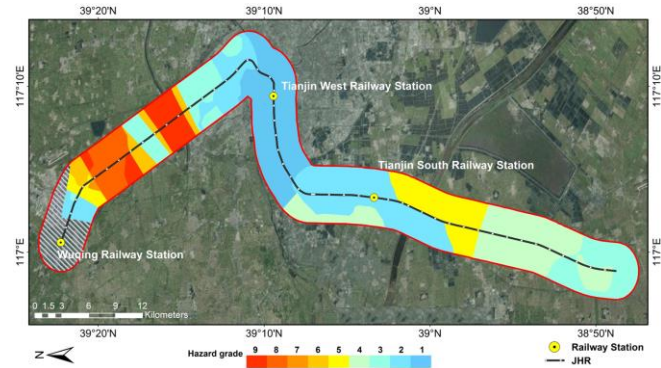

Fig. 10. Hazardous grading of JHR (2008-2009). Background image: Google Map.

The hatched portions denote areas without data and the colors from red to blue indicate the hazardous grades from serious to slight. The segment near Shuangjie Town (expressed as red) in the JJR suffered the most serious subsidence hazard, followed by a north section (expressed as orange) near Wuqing Railway Station. In the JHR, the segment (expressed as yellow) near Dafengdui Town is also worthy of attention in the maintenance and management.

B. Shanghai-Hangzhou High-speed Railway

1) 2D Deformation Along the Route

The linear LOS deformation rates of the HHR from ASAR and TSX (2008-2010) are showed in Fig. 11(a) and (b), where the subsidence section A near an industrial zone was identified. As parts of the roadbed are rough targets for the X-band (3.1 cm), much more PTs can be detected in the TSX results. The Eq. (15) - (18) were applied to estimate the vertical and west-east velocities along the track (see Fig. 12(a) and (b)). The 2D deformation rates indicated that the vertical velocities along the route are the dominant components while the west-east velocities are much smaller (within ±4 mm/yr). In the subsidence section A, strong vertical velocities were detected while the behaviors in west-east direction were less pronounced.
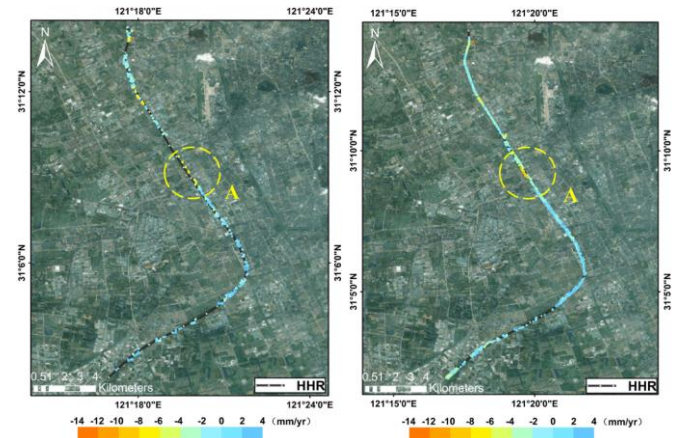
(a) LOS deformation rate from ASAR   (b) LOS deformation rate from TSX
Fig. 11. LOS deformation rate map of HHR (2008-2010). Background image: Google Map.
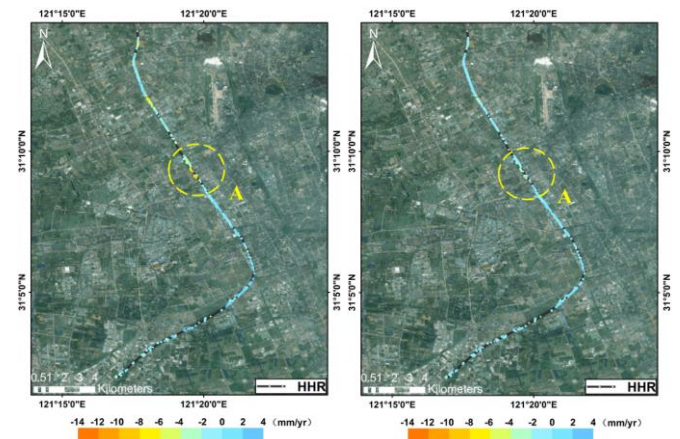
(a) Vertical deformation rate   (b) West-east deformation rate
Fig. 12. Vertical and west-east deformation rate maps of HHR combining ASAR and TSX images (2008-2010). Background image: Google Map.
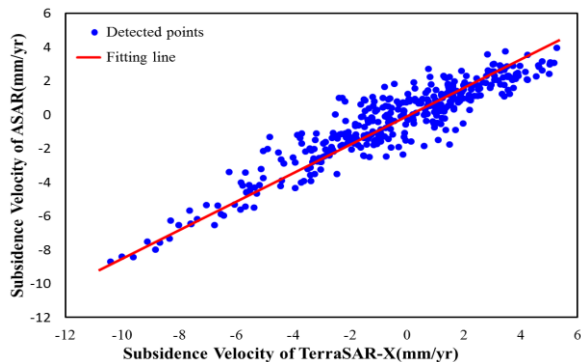

Fig. 13. Deformation rate scatter plot of TSX versus ASAR (2008-2010)

Hongqiao Hub, the largest hub in the world, creates a precedent of zero transfer between multiple transportations with annual passenger throughput of 95 million. It is therefore essential to detect its stability regularly. The vertical deformation rate maps of Hongqiao Hub from the two TSX datasets are illustrated in Fig. 14(a) and (b). Since Hongqiao hub was under construction from 2008 to 2010, very few points are selected in Fig. 14(a) while much more points on the buildings and tracks are selected in Fig. 14(b). Lots of PTs are identified on the old No.1 runway but only a few on the new

No.2 runway. According to the google map, the No.1 runway is black while the No.2 runway is white. A reasonable explanation may be that they are constructed by different materials, which would indeed affect the density of PTs. The subsidence mainly occurred on the Shenghong mansion, No.2 terminal building and freight station of Hongqiao Airport, and the track around Hongqiao Railway Station, while the runways and Hongqiao Railway Station building remain stable. This may be related to the different underlying geological conditions, building foundation types, and ground loads of these structures.
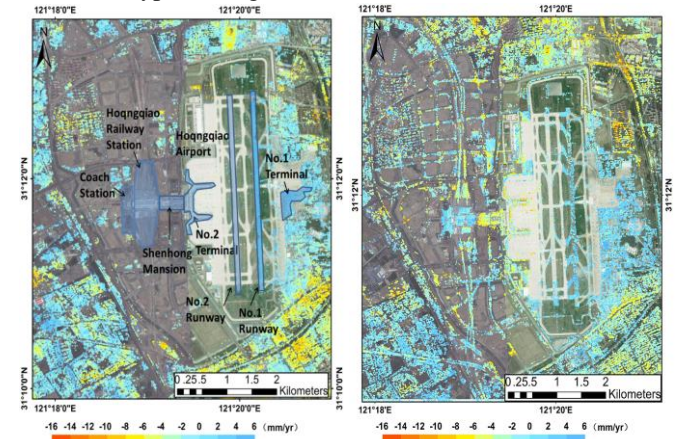
(a) From 2008 to 2010   (b) From 2011 to 2012
Fig. 14. Deformation rates of Hongqiao Hub during two different periods. Background image: Google Map.

Although the ground survey data is not available along the route, the overall subsidence pattern of TSX results is consistent with the leveling results in the coverage [33]-[34]. Besides, the subsidence velocities from the TSX and ASAR images show consistent deformation patterns. The scatter plot of their velocities comparison in Fig. 13 demonstrated that the two independent results agreed well with each other.

2) Thermal Dilation Analysis
We estimated the thermal dilation by TSX datasets due to its higher sensitivity to the thermal dilation. The estimated TDPs of a buffer zone are displayed in Fig. 15. Most objects, including the runways and railway embankment, had no displacements associated with temperature variations. However, periodical thermal dilations were observed in some suburb areas with intensive industrial plants.

As the geometry of the building is low in height (30 m in the central and 20 m in both sides) and much more elongated (length: 1 km, width: 220 m), its thermal dilation pattern is similar to a linear structure, with displacements away and toward the satellite periodically. Four differential interferograms of this building with different temperature gaps and close normal baselines are showed in Fig. 16. It is widely believe that fringes caused by height differences rely on the normal baseline while those caused by thermal dilation are mainly related to the temperature differences. From Fig.16 we can see that, the periodical distortions, overlaid on the building's roof, showed a quickly change in color in the differential interferograms with large temperature gaps (see Fig. 16(a) and (d)). However, the colorful stripes change slowly in Fig. 16(b) and (c) which have smaller temperature differences.

Therefore, these periodical fringes can probably be explained as the thermal dilation of building [35] due to the temperature difference of the differential interferogram.
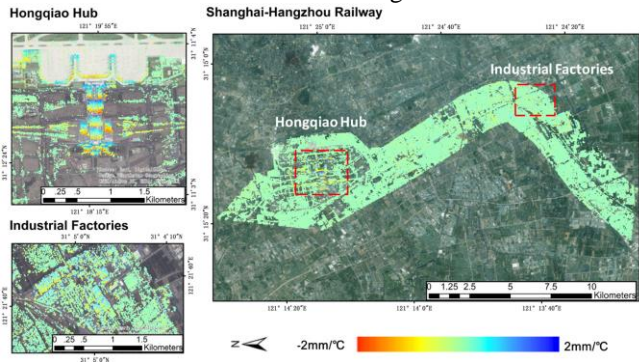

Fig. 15. Thermal dilation map of HHR and Hongqiao Hub (2011-2012). Background image: Google Map.

(a) 20110916-20120310
$B_n = \mathbf{36}$m; $\Delta T = \mathbf{18.9}$℃

(b) 20120104-20120310
$B_n = \mathbf{48}m$; $\Delta T = -\mathbf{4.7}$℃

(c) 20120206-20120310
$B_n = \mathbf{56}$m; $\Delta T = -\mathbf{3.1}$℃

(d) 20120720-20120310
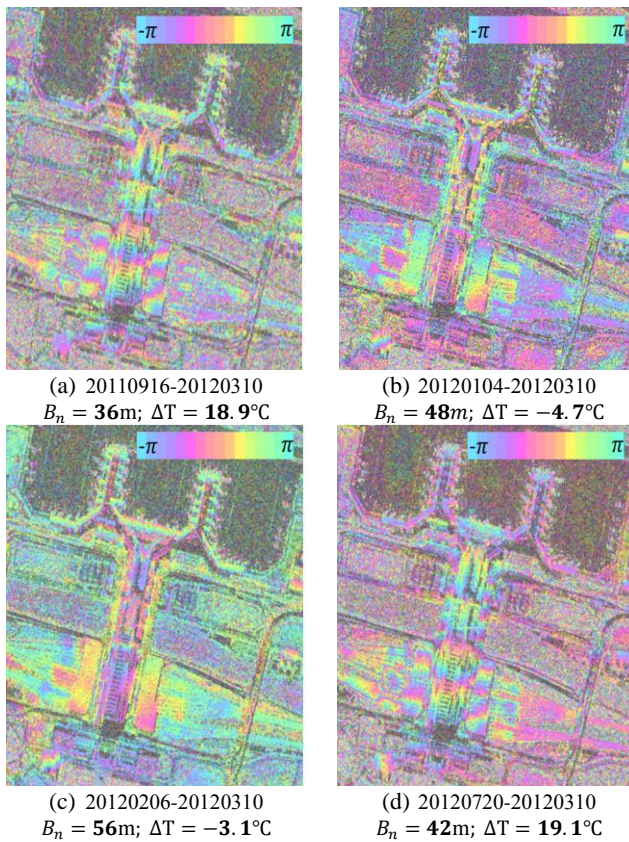$B_n = \mathbf{42}$m; $\Delta T = \mathbf{19.1}$℃

Fig. 16. Differential interferograms of Hongqiao Hub (2011-2012)

By using a least square fitting between the residual phases and the temperature variations, the thermal dilation can be effectively extracted. From the enlarged map of the buildings in the top left of Fig. 15, we can see that the spatial distribution of the TDPs coincided with the colorful stripes, providing rich information about the static structure of the object. These parameters ranged from -2 to 2 mm/℃ in about 200 m. Assuming the thermal dilation mainly propagated in the west-east direction (the building's longitudinal direction) linearly, a TEC of $9.8 \cdot 10^{-6}/℃$ can be estimated by Eq. (9), which is exactly a physical property for the steel reinforced concrete（$8\sim12 \cdot 10^{-6}/℃$）. This parameter, if in a longer extent, can discriminate different types of materials. Taking 10

points on the building, the scatter plot of the average displacements and corresponding temperature differences (see Fig. 17) showed an excellent linear relationship. The RMSE of the thermal dilation linear fitting model is 1.027 mm.
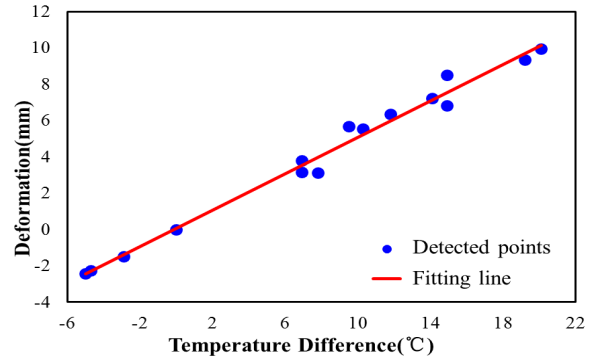

Fig. 17. Scatter plot for residual deformation versus temperature difference of Hongqiao Hub (2011-2012)

3) Hazardous Grading Evaluation

Using the same grading standards described in table V, the hazardous grades along the HHR from 2008 to 2010 retrieved by ASAR and TSX measurements are illustrated in Fig. 18 and Fig. 19 respectively. Hazardous grades from one to nine indicate the hazard becoming increasingly serious. Comparing Fig. 18 and Fig. 19, the overall distributions of the hazardous grades are almost the same. As the construction of Hongqiao Hub resulted in decorrelation, the hazardous grades were null on it. A segment near Jiamin elevated road in the west of Hongqiao Hub (expressed as orange) suffered the highest risk, followed by the segment A expressed as orange and yellow. However, as TSX has a higher resolution than ASAR, a few areas in Hongqiao Hub can still be detected by TSX, and thus, the hazardous grades pattern of TSX can provide more accurate information along the track. Therefore, we can infer that TSX observations are more appropriate for high-speed railway monitoring than those of ASAR.
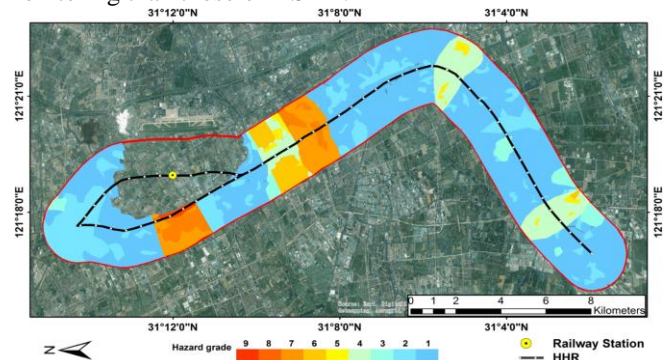

Fig. 18. Hazardous grading of HHR by ASAR (2008-2010). Background image: Google Map.

The hazardous grades from 2011 to 2012 are showed in Fig. 20 where most segments remained stable and safety. However, the segments near Hongqiao Hub and subsidence area A expressed as red and orange suffered from severe damage. Therefore, special attention and continuous monitoring are essential for these segments, especially for the major municipal engineering like the Hongqiao Hub.
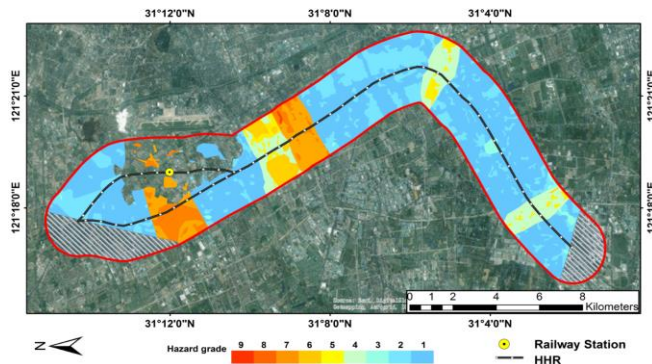
Fig. 19. Hazardous grading of HHR by TSX (2008-2010). Background image: Google Map.
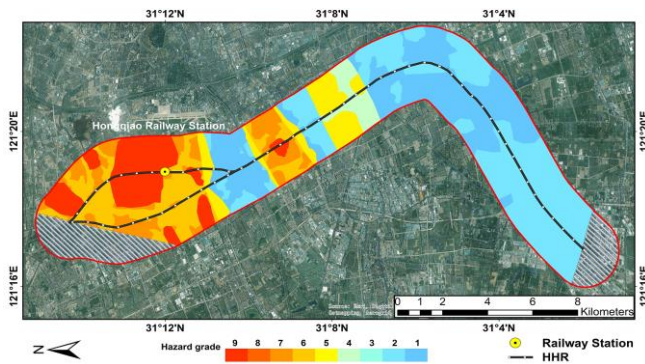

Fig. 20. Hazardous grading of HHR by TSX (2011-2012). Background image: Google Map.

V. CONCLUSION AND OUTLOOK

In this study, we investigated the potential of an improved PSI analysis approach for structural health and stability assessment of high-speed railways. Our results show that the spatial-temporal strategy can effectively identify high-density PTs and facilitates the calculation of reliable results. The deformation patterns along the tracks are strongly related to human activities, geological settings, and loading scenarios. For example, the groundwater exploitation has a significant impact on the stability of subsidence segments near the town areas along the JJR and JHR lines. Hazardous grades were divided into nine levels to identify risky segments by combining the significant indicators of the smoothness including subsidence velocity, gradient, and thermal dilation. Although the maximum subsidence gradients along the tracks are still within the specifications, the accelerated growth in cumulative subsidence, nevertheless, might affect the safe operation of high-speed trains over time.

Thermal dilation is also a significant component of the total deformation. A least square fitting of the residual phase obtained by iterative spatial-temporal filtering with respect to temperature difference is used to estimate the TEC of the materials. Most parts of the tracks showed negligible thermal dilation while a few segments have visible thermal dilation. The negative TDPs are related to the seasonal variation in the subgrade and groundwater level. The thermal dilation at the Hongqiao Hub was propagated in the horizontal direction, providing rich information about its static structure. This was verified by reversing a TEC consistent with the physical property of steel reinforced concrete.

The linear deformation rates in the vertical and east-west directions along the HHR were inverted from ascending ASAR and descending TSX observations. The 2D deformation velocity distribution indicated that the deformation along the track is mainly in the vertical direction. The subsidence segment A with a predominantly vertical velocity and a negligible west-east velocity confirmed this conclusion. Moreover, the cross-validation between TSX and ASAR results was highly consistent.

Such observations of engineering-scale deformation on high-speed railways can aid the evaluation of the stability of railway structures in a fast and reliable way over wide area. These observations also provide useful guidance and reference for transport operators by identifying the risky segments which require field inspection. As the high-speed railways come into operation, we not only need to solve the problem of current differential settlement, but also must consider how to prevent such issues from arising in the first place. On the one hand, measures of strengthening the track adjustment performance and controlling the exploitation of groundwater should be implemented to restrain the development of differential settlement. On the other hand, based on the existing monitoring network, future systems for subsidence detection on high-speed railways will require close collaboration among multi-disciplines including InSAR remote sensing, geophysics, hydrogeology, and civil engineering.

REFERENCES

[1] L. Ge, X. Li, H. Chang, et al, "Impact of ground subsidence on the Beijing–Tianjin high-speed railway as mapped by radar interferometry," *Annals of GIS*, vol. 16, no.2, pp. 91-102, Jun. 2010.
[2] G. Duan, H. Gong, H. Liu, et al, "Monitoring and analysis of land subsidence along Beijing-Tianjin Inter-city railway," *J. Indian Soc. Remote Sens.*, pp. 1-17, Jan. 2016.
[3] H. Lan, L. Li, H. Liu, et al, "Complex urban infrastructure deformation monitoring using high resolution PSI," *IEEE J. Sel. Topics Appl. Earth Observ. Remote Sens.*, vol. 5, no. 2, pp. 643-651, Apr. 2012.
[4] L. Chang, R. Dollevoet, and R. F. Hanssen, "Nationwide railway monitoring using satellite SAR interferometry," *IEEE J. Sel. Topics Appl. Earth Observ. Remote Sens.*, vol. pp, no. 99, pp.1-9, Jun. 2016.
[5] L. Chang, "Monitoring civil infrastructure using satellite radar interferometry," Ph.D. dissertation, Dept. Geosci. Remote Sens., Delft Univ. Technology, Delft, 2015.
[6] Q. Zhao, A. Pepe, W. Gao, et al, "A DInSAR investigation of the ground settlement time evolution of ocean-reclaimed lands in Shanghai," *IEEE J. Sel. Topics Appl. Earth Observ. Remote Sens.,* vol. 8, no. 4, pp. 1763-1781, Apr. 2015.
[7] A. Ferretti, C. Prati, and F. Rocca, "Permanent scatterers in SAR interferometry," *IEEE Trans. Geosci. Remote Sens.*, vol. 39, no. 1, pp. 8–20, Jan. 2001.
[8] P. Beradino, G. Fornaro, R. Lanari, and E. Sansosti, "A new algorithm for surface deformation monitoring based on small baseline differential SAR interferograms," *IEEE Trans. Geosci. Remote Sens.*, vol. 40, no. 11, pp. 2375–2383, Nov. 2002.

[9] C. Werner, U. Wegmüller, T. Strozzi, and A. Wiesmann, "Interferometric point target analysis for deformation mapping," *in Proc. IEEE Int. Geosci. Remote Sens. Symp.*, pp. 4362–4364, Jul. 2003.

[10] X. Shi, L. Zhang, T. Balz, et al, "Landslide deformation monitoring using point-like target offset tracking with multi-mode high-resolution TerraSAR-X data," I*sprs J. Photogramm. Remote Sens.* vol. 105, pp. 128-140, 2015.

[11] L. Chang, R. Dollevoet, R. F. Hanssen, "Railway infrastructure monitoring using satellite radar data," *Int. J. of Railway Technol.* vol. 3, no.2, pp. 79-91, 2014.

[12] F. Chen, H. Lin, Z. Li, et al, "Interaction between permafrost and infrastructure along the Qinghai–Tibet railway detected via jointly analysis of C- and L-band small baseline SAR interferometry," *Remote Sens. Environ.*, vol. 8, no. 123, pp. 532-540, May 2012.

[13] X. Shi, M. Liao, T. Wang, et al, "Expressway deformation mapping using high-resolution TerraSAR-X images," *Remote Sens. Lett.*, vol. 5, no. 2, pp. 194-203, Jan. 2014.

[14] M. Crosetto, O. Monserrat, M. Cuevas, et al, "Measuring thermal expansion using X-band Persistent Scatterer Interferometry," *Isprs J. Photogramm. Remote Sens.*, vol. 100, pp. 84-91, May 2014.

[15] M. Lazecky, I. Hlavacova, M. Bakon, et al, "Bridge displacements monitoring using space-borne X-band SAR interferometry," *IEEE J. Sel. Topics Appl. Earth Observ. Remote Sens.*, May. 2016.

[16] Q. Luo, D. Perissin, H. Lin, et al, "Subsidence monitoring of Tianjin suburbs by TerraSAR-X Persistent Scatterers Interferometry," *IEEE J. Sel. Topics Appl. Earth Observ. Remote Sens.,* vol. 7, no. 5, pp. 1642-1650, May. 2014.

[17] P. Daniele, Z. Wang, H. Lin, "Shanghai subway tunnels and highways monitoring through Cosmo-SkyMed Persistent Scatterers," *Isprs J. Photogramm. Remote Sens.*, vol. 73, pp. 58-67, Sep. 2012.

[18] A. Hooper, "Persistent Scatterer Radar Interferometry for crustal deformation studies and modeling of volcanic deformation," Ph.D. dissertation, Dept. Geophysics, Stanford Univ. Palo Alto, America, 2006.

[19] A. Hooper, H. Zebker, P. Segall, et al, "A new method for measuring deformation on volcanoes and other natural terrains using InSAR persistent scatterers," *Geophys. Res. Lett.*, vol. 31, no. L23611, 2004.

[20] R. F. Hanssen, *Radar Interferometry: Data Interpretation and Error Analysis*. Dordrecht, Netherland: Kluwer, 2001.

[21] A. Ferretti, C. Prati, F. Rocca, "Nonlinear subsidence rate estimation using permanent scatterers in SAR interferometry," *IEEE Trans. Geosci. Remote Sens.*, vol. 38, no.5, pp.2202-2212, Sep. 2000.

[22] M. Liao, H. Jiang, Y. Wang, T. Wang, L. Zhang, "Improved topographic mapping through high-resolution SAR interferometry with atmosphere effect removal," *Isprs J. Photogramm. Remote Sens.*, vol. 80, pp. 72-79, Apr. 2013.

[23] J. Hu, Z. Li, J. Zhu, et al. "z," *Science China: Earth Science,* vol. 53, no. 4, pp. 550-560, 2010.

[24] k. Dai, G. Liu, Z. Li, et al. "Extracting vertical displacement rates in Shanghai (China) with multi-platform SAR images," *Remote Sens.,* vol. 7, no. 8, pp.9542-9562, 2015.

[25] J. Hu, Z. Li, Q. Sun, et al. "Three-dimensional surface displacements from InSAR and GPS measurements with variance component estimation," *IEEE Geosci. Remote Sens. Lett.*, vol. 9, no.4, pp. 754-758, 2012.

[26] M. Yang, M. Liao, X. Shi et al. "Land subsidence monitoring by joint estimation of multi-platform time series InSAR observations," *Geomatics and Information Science of Wuhan University,* vol. 38, no. 3, pp. 266-269, Oct. 2016.

[27] K. Dai, G. Liu, B. Yu, et al, "Detecting subsidence along a high speed railway by ultrashort baseline TCP-InSAR with high resolution images," *ISPRS - International Archives of the Photogrammetry*, pp. 61-65, 2013.

[28] T. Li, H. Zhang, C. Wang, et al, "Comparison of Beijing-Tianjin intercity railway deformation monitoring results between ASAR and PALSAR data," *Geoscience and Remote Sensing Symposium (IGARSS), IEEE International* IEEE, pp. 3514-3517, Jul. 2010.

[29] G. Liu, H. Jia, R. Zhang, et al, "Exploration of subsidence estimation by persistent scatterer InSAR on time series of high resolution TerraSAR-X images," *IEEE J. Sel. Topics Appl. Earth Observat. Remote Sens.*, vol. 4, no. 1, pp. 159–169, Mar. 2011.

[30] B. Hu, J. Zhou, J. Wang, et al, "Risk assessment of land subsidence at Tianjin coastal area in China," *Environ. Earth Sci.*, vol. 59, no. 2, pp. 269–276, 2009.

[31] G. Li, Z. Xu, S. S, et al, "The influence of surface subsidence on construction of High-speed railway in North China Plain and its countermeasures," *J. Railway Engineering Society*, vol. 24, no. 8, pp. 7-12, 2007.

[32] R. Wang, Y. Yang, F. Tian, et al, "Construction of a monitoring system for regional land subsidence affecting high-speed railways," *Shanghai Land & Resources*, vol. 35, no. 2, pp. 17-20, 2014.

[33] X. Qin, M. Yang, H. Wang, et al, "Application of high-resolution PS-InSAR in deformation characteristics probe of urban rail transit," *Acta Geodaetica et Cartographica Sinica*, vol. 45, no. 6, pp.713-721, Jun. 2016.

[34] X. Qin, M. Yang, M. Liao, et al, "Exploring temporal-spatial of shanghai road networks settlement with multi-temporal PSInSAR technique," *Geomatics and Information Science of Wuhan University*, vol.42, no.2, pp. 170-177, Feb. 2017

[35] M. Eineder, N. Adam, R. Bamler, et al. "Spaceborne spotlight SAR interferometry with TerraSAR-X." *IEEE Trans. Geosci. Remote Sens.*, vol. 47, no. 5, pp. 1524-1535, 2009.
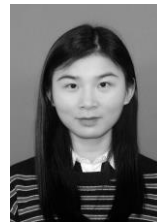
Xiaoqiong Qin received the B.Eng. degree in Geographic Information Engineering from Southeast University, Nanjing, China, in 2013. She is currently working toward the Ph.D. degree in Photogrammetry and Remote Sensing from State Key Laboratory of Information Engineering in Surveying, Mapping and Remote Sensing (LESMARS), Wuhan University, China.

Her current research interests include time-series InSAR techniques for structure health monitoring of infrastructures, and land subsidence monitoring and analysis in urban area.

Mingsheng Liao received the B.S. degree in Electronic Engineering from Wuhan Technical University of Surveying and Mapping (WTUSM), Wuhan, China, in 1982, the M.A. degree in Electronic and Information Engineering from Huazhong University of Science and Technology, Wuhan, China, in 1985, and the Ph.D. degree in Photogrammetry and Remote Sensing from WTUSM, Wuhan, China, in 2000.

He is working at the LIESMARS, Wuhan University, where he became a Professor in 1997. He is the PI of several projects funded by the Ministry of Science and Technology (MOST) China and the Natural Science Foundation of China. He is also the Co-PI of the ESA-MOST cooperative Dragon I (2004-2008), II (2008-2012), III (2012-2016) and IV (2016-2020) projects. He has published more than 60 peer-reviewed journal papers and several book chapters focused on InSAR techniques and applications. His research interests include remote sensing image processing and analysis, algorithms for interferometric SAR, integration and fusion of multi-source spatial information and applications of remote sensing data.
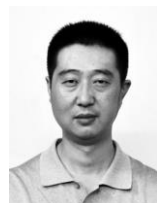
Lu Zhang received the B.Eng. and M.Eng. degrees in Computer Science and Technology from Wuhan University of Hydraulic and Electrical Engineering, Wuhan, China, in 1997 and 2000, and the Ph.D. degree in Photogrammetry and Remote Sensing from Wuhan University, Wuhan, China, in 2005. From 2005 to 2007 he has been a Post-Doctoral Research Fellow at the Institute of Space and Earth Information Science, Chinese University of Hong Kong.

Since 2007 he has been working at LIESMARS and become a full Professor in 2013. His research is focused on SAR interferometry as well as remote sensing classification and change detection. He has been involved in several research projects funded by NSFC and MOST. In recent years he has published about 30 peer-reviewed scientific papers.

Mengshi Yang received the B.Eng. degree in Geomatics Engineering from Central South University, Changha, China, in 2012. She is currently working toward the Ph.D. degree in the Department of Geoscience and Remote Sensing of Delft University of Technology, the Netherlands and LESMARS of Wuhan University, China.

Her current research interests include the high-precision geo-location of SAR scatterers, the collaboration between InSAR and Lidar data, and InSAR time series technique for civil-protection.